Materials Science & Engineering C 118 (2021) 111372

Contents lists available at ScienceDirect

Materials Science & Engineering C

journal homepage: www.elsevier.com/locate/msec

Biomimetic micellar mesoporous silica xerogel performs superior nitrendipine dissolution, systemic stability and cellular transmembrane transport

Qiankun Jiang, Lingqiong Wu, Yue Zheng, Xiaojie Xia, Ping Zhang, Tong Lu, Jing Li*

School of Pharmacy, Shenyang Medical College, Shenyang, China

ARTICLE INFO

Keywords:
Biomimetic micellar mesoporous silica xerogel
Nitrendipine dissolution
Systemic stability
Cellular transmembrane transport

ABSTRACT

To combine the advantages of micelles and biomimetic silica materials, biomimetic micellar mesoporous silica xerogel (BM-SX) was initially established, biomimetic silica xerogel (B-SX) was also studied as control and nitrendipine (NDP) was taken as model drug. The content mainly focused on drug dissolution, systemic stability and cellular transmembrane transport of NDP loaded B-SX and NDP loaded BM-SX. With extra mesopores formed due to HPMC E50 micelles, the mean pore diameter, surface area and pore volume of BM-SX were all larger than B-SX. After loading NDP into the two carriers, crystal NDP changed to amorphous phase, leading to enhanced NDP dissolution. BM-SX presented superior abilities not only for its higher drug dissolution compared to B-SX but also for its capacity in remaining high amorphous drug phase and therefore no drug dissolution reduction can be observed. The dynamic contact angle result confirmed the strong power of HPMC E50 micelles in maintaining amorphous NDP in the carrier to improve high systemic stability. Both B-SX and BM-SX could increase drug absorption permeability and exert function as drug efflux inhibitor to inhibit the efflux effect of p-gp drug pump and promote NDP absorption and transport, and BM-SX was superior owing to micelles in the system.

1. Introduction

In drug delivery industry, micelles have been given great interest owing to their advantages, including well defined molecular structures, assembling behaviours, well stabilized drug solution, large-scale production and stable clinical performance of the formulations [1–3]. Generally, micelle that consists of one hydrophilic shell and one hydrophobic core can be divided into two main categories: hydrophobically assembled micelles and polyion-complex micelles. Hydrophobically assembled micelles are formed by amphiphilic copolymers with a hydrophobic block and a hydrophilic block, such as poly (ethylene glycol). The polyion-complex micelles applied charged polymer blocks, typically as poly(ethyleneimine), poly(aspartic acid) and poly(L-lysine), to mainly deliver therapeutic nucleic acids and oppositely charged protein drugs [4,5]. Polymer can form micelle structure when the lowest concentration reaches critical micelle concentration (CMC). When the concentration decreases below CMC, the micelle structures are disintegrated into unimers. According to many researches, CMC can be mainly decided by themolecular mass (size) and the hydrophobicity of copolymers [6]. Micelles can be used to solubilize and deliver poorly water-soluble drugs. Furthermore, micelles can permeate through the leaky inflamed blood vessels due to the highly water-bound barrier created by hydrophilic corona. Third, micelles can realize both diagnosis and therapy. Finally, surface modification of micelles by specific ligands can improve targeting efficiency and decrease the toxicity [26]. However, there are three major hurdles for translating polymer micelles from academic research to clinical application, including the low drug loading efficiency, the poor blood stability after injection, and the difficulty in transporting through cell membranes.

Seen from diatoms and sponge spicules in the living world, silica can be formed with impressive morphologies, structures, and physical properties under ambient conditions. Biosilicification is defined as the movement of silicic acid from environments with concentration lower than its solubility and accumulated for subsequent deposition as amorphous hydrated silica [7,8]. The advantages of biological silica formation have attracted great attention, including ornate and hierarchical structures, mild pH, ambient temperatures, environmental friendly, controlled and involvement of organic components. Biomimetic silica can be obtained by applying several kinds of templates,

* Corresponding author at: No. 146 Huanghe North Street, Shenyang, Liaoning Province, China.
E-mail address: dddefghijklmn@163.com (J. Li).

https://doi.org/10.1016/j.msec.2020.111372
Received 10 October 2019; Received in revised form 7 April 2020; Accepted 20 July 2020
Available online 07 August 2020
0928-4931/

including polyamine [9], protein, enzyme, etc. [10]. Biosilica presents hierarchical particles and pores in the range of nanometres to micrometres. Its structure is extremely hard to be achieved in synthetic process, especially under mild conditions. Prior to the development of bioinspired silica synthesis, silica formation at near-neutral working conditions (pH and room temperature) is rarely accomplished since the rate of hydrolysis is the lowest at pH = 7 with gelation taking longer than at any other pH. Typically, silica and silicates formed after going through sol-gel process at low temperature. Sol-gel process uses alkoxysilanes (toxic but also possess limited solubility in water) as silica precursors and mixture of water and alcohol as solvent. In a word, biosilica forms in all-aqueous environments and non-toxic silica in natural water.

Mesoporous silica materials have been long recognized as effective drug carrier and used to establish a profound of drug delivery systems [11,12]. To combine the advantages of micelles and biomimetic silica materials, biomimetic micellar mesoporous silica xerogel (BM-SX) was established and biomimetic mesoporous silica xerogel (B-SX) was also studied as control. Nitrendipine (NDP), a poorly water soluble drug with solubility about 1.9–2.1 μg/mL, is applied for treating cardiovascular disorders. NDP was used as model drug to study the advantages of BM-SX in loading poorly water soluble drug. Drug dissolution, systemic stability and cellular transmembrane transport of NDP loaded B-SX and NDP loaded BM-SX were mainly focused. The overall elucidation of advantages of BM-SX has great value for promoting the application of mesoporous silica materials.

2. Materials and methods

2.1. Materials

Tetramethoxysilane (TMOS) was purchased from Aladdin (Shanghai, China). Hydroxypropyl methyl cellulose E50 (HPMC E50) was provided by Anhui Sunhere Pharmaceutical Excipients Co. Ltd. All other chemical were of reagent grade and deionized water was prepared by ion exchange.

2.2. Preparation of BM-SX and B-SX

Prior to experiment, 50 mg/mL HPMC E50 solution and 1.0 wt% PEIs solution [7] were prepared by dissolving them using deionized water. The brief preparation process of BM-SX was described as follows. 0.1 mL PEIs solution was mixed with 0.1 mL HPMC E50 solution. Afterwards, 0.5 mL TMOS was added into the above mixture and dispersed uniformly. The system was left at ambient condition statically until the formation of wet gel and finally dried to obtain xerogel. B-SX was prepared using the similar working process except for adding HPMC E50. It should be noted that 50 mg/mL HPMC E50 was chosen because its formation of biomimetic silica gel was the fastest among a serious concentration of HPMC E50 (30 mg/mL: about 8 h 32 min; 40 mg/mL: about 8 h 16 min; 50 mg/mL: about 6 h 45 min, 60 mg/mL: about 7 h 38 min). The reason may be because low concentration of HPMC E50 was not favorable for accelerating silica polycondensation while too high concentration of HPMC E50 reduced silica polycondensation due to high viscosity of the system caused by its high concentration.

2.3. Drug loading process

NDP was loaded into BM-SX or B-SX using in situ loading method. 0.1 mL PEIs solution was mixed with 0.1 mL HPMC E50 solution. Afterwards, 1.0 mL drug solution was added and then 0.5 mL TMOS was added into the above mixture. The system was agitated uniformly and left at ambient condition statically until the formation of wet gel and finally dried to obtain xerogel. Drug loading efficiency was calculated by subtracting the loaded drug from carrier using UV-1120 (Shimadzu, Japan) at 256 nm.

$$\text{Drug loading capacity (\%)} = (\text{W drug in carrier/W carrier}) \times 100$$

2.4. Critical micelle concentration (CMC)

Pyrene with solubility of about 10^{-7} mmol/L in water shows its fluorescence peaks at 373, 379, 384, 390, 395 nm and 480 nm [13]. The value of I3/I1 (the ratio of the fluorescence intensity at 373 nm to the fluorescence intensity at 384 nm) is determined by the polarity of the environment. The smaller I3/I1, the stronger polarity of system it is. Pyrene is solubilized by surfactant and can enter into hydrophobic core surrounded by long carbon chain with small polarity of surfactant. Therefore, the CMC of surfactant can be determined by mutation of I3/I1 value [14].

Herein, pyrene solution (6×10^{-6} mol/L) and various excipient aqueous solution were prepared before the experiment. 100 μL pyrene solution was dried in EP tube and excipient aqueous solution was added. The sample was shaken at 100 rpm at 37 °C for 12 h. 50 μL sample was withdrawn into 96-well plate and was tested using ELIASA with 335 nm as λex, 373 nm and 384 nm as λem respectively to obtain I3 and I1.

Molar Solubilization Ratio (MSR) is used to describe the solubility of a given solute in surfactant solution [15].

$$R = (S_t - S_{CMC})/(C_t - C_{CMC}) \quad (1\text{-}1)$$

where R stands for MSR, Ct is the concentration above CMC, S_t and S_{CMC} are designed for the concentration of surfactant solution and the apparent solubility at CMC. The image with concentration of surfactant solution as horizontal axis and drug concentration as vertical axis was drawn. The slope of this image is MSR.

2.5. Morphology and porous structure of carriers

2.5.1. Scanning electron microscopy (SEM)

Morphology of carriers can be reflected using SURA 35 field emission scanning electron microscope (ZEISS , Germany). Samples were mounted onto metal stubs using double-sided adhesive tape and sputtered with a thin layer of gold under vacuum.

2.5.2. Nitrogen adsorption/desorption analysis

Nitrogen adsorption/desorption of carriers were studied by nitrogen adsorption and desorption measurement using V-Sorb 2800P (app-one, China). All samples were degassed at 50 °C vacuum drying for sufficient time prior to analysis to remove adsorbed water.

2.6. Differential scanning calorimeter (DSC)

Thermal analysis was conducted by utilizing differential scanning calorimeter (DSC, Q1000, TA Instrument, USA). Samples were placed in pierced aluminum pans and heated from 30 to 300 °C at a scanning rate of 10 °C/min under nitrogen protection.

2.7. Drug release

In vitro dissolution was carried out using stirring method (100 rpm, 37 °C) with a RC806D dissolution tester (Tianjin, China). Samples were exposed to enzyme-free simulated gastric fluid (pH 1.0 hydrochloric acid). At predetermined time intervals, 5 mL sample medium was withdrawn and replaced with an equivalent amount of fresh medium to maintain a constant dissolution volume. After going through 0.45 μm microporous membrane, the sample medium was analyzed using UV-1120 (Shimadzu, Japan) at the wavelength of 256 nm.

2.8. Wetting property

Contact angle measurement was applied to reveal the wetting property of samples. Briefly, 200 mg powdered sample was compressed using a circular stainless steel punch and die. 2 μL dissolution medium was put on the compressed plate and contact angle was measured by automatic contact angle meter model JCY series (Shanghai, China).

2.9. Storage stability

High storage stability is a crucial parameter for preparation products. Moisture absorption experiment was conducted by placing tablet samples in desiccator with humidity of 92.5% for 5d or 10d. Then samples were withdrawn and measured the dynamic contact angle.

2.10. Cellular toxicity and transmembrane transport

Caco-2 cell suspension was inoculated at a density of 1.0×10^5/mL on a 12-well Transwell® culture plate, and the culture solution was added on the substrate side. The culture base was Dulbecco's Modified Eagle's Medium with 1% non-essential amino acids, 1% L-glutamine, 100 U/mL penicillin, 100 mU/mL streptomycin and 10% fetal bovine serum. Culture was stored in an environment of 37 °C and 90% (5%CO_2) relative humidity. Culture solution was changed after inoculation for 24 h to remove residue and dead cells. Next, the culture solution was changed for several times. After caco-2 cells formed a tight and complete single-cell layer on the Transwell® culture plate, cell culture medium was discarded, HBSS (pH 7.4) solution at 37 °C was added into each hole, cell surface was washed to remove the attachment, and HBSS solution was added and cultured in an incubator at 37 °C for 30 min.

The cellular toxicity of BM-SX and B-SX was evaluated by MTT assays. Briefly, Caco-2 cells were grown for 12 h and then were exposed to various concentrations of samples and further incubated for 48 h. The culture medium with sample was replaced by 100 μL fresh medium without fetal bovine serum, and then 20 μL sterile MTT solution (5 mg/mL) was added to each well, and incubated for additional 4 h at 37 °C. The media was removed, and 150 mL DMSO was added to each well to dissolve MTT formazan. The absorbance was measured at 570 nm using BioRadicroplate reader (Model 500, USA). The cell viability rate was calculated finally.

To investigate the effect of p-gp specific inhibitor cyclosporine A (CsA) on the drug transport in the caco-2 monolayer cell model, cells were first treated with solution containing 12 mg/L CsA for 2 h, the monolayer cells were removed from both sides of the solution, and the cells were washed with HBSS. Drug transmembrane transport from AP side to BL side: drug, or drug with CsA, or drug loaded carrier solution was added to the AP side as a feeding pool, and blank HBSS (pH 7.4) solution was added to the BL side as a receiving pool. For BL to AP drug transmembrane transport, drug, or drug with CsA, or drug loaded carrier solution was added to BL as a feeding pool, and a blank HBSS solution was added to AP as a receiving pool. Transwell® culture plates were placed on a constant temperature shaking table at 37 °C and vibrated at 50 rpm. At 20, 40, 60, 90 and 120 min, 100 μL of the receiving solution was absorbed, and 37 °C blank HBSS solution was added at the same time. The experiment was repeated three times. The drug concentration in receiving liquid was measured.

Apparent permeability coefficient (Papp) was calculated according to the following equation.

$$\text{Papp} = (dQ/dt)/(A \times C_0)\ \text{cm/s} \quad (1\text{-}2)$$

Among this equation, Papp stands for drug transport ability, dQ / dt means drug transport amount per unit of time (mol·s^{-1}), A stands for surface area (1.13 cm^2), C_0 is the original drug concentration. Efflux ratio (ER) can be obtained by the following equation.

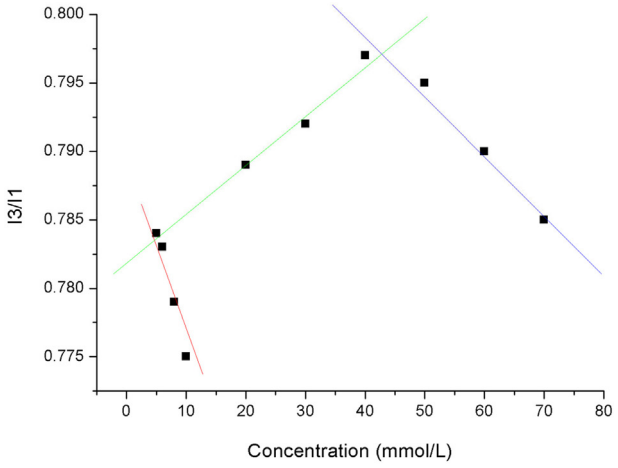

A

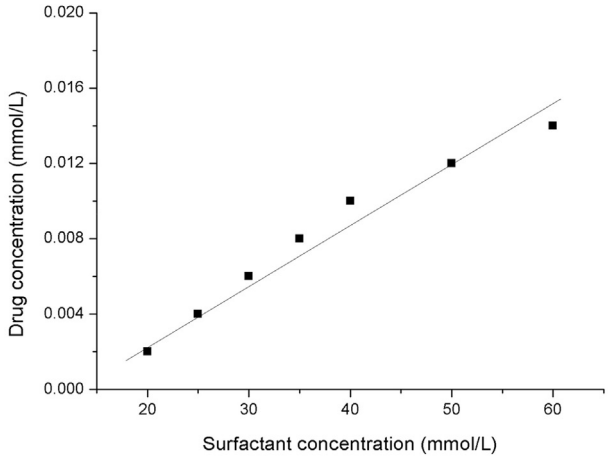

B

Fig. 1. A, CMC of HPMC E50 solution; MSR of HPMC E50 solution.

$$\text{ER} = \text{Papp (BL} \rightarrow \text{AP)/Papp (AP} \rightarrow \text{BL)} \quad (1\text{-}3)$$

ER reflects drug efflux capacity, Papp (BL → AP) is secretory apparent permeability coefficient, Papp (AP → BL) stands for absorption apparent permeability coefficient.

3. Results and discussions

3.1. Micellar properties

According to Fig. 1, the CMC of HPMC E50 was 24.8 mmol/L. Since the concentration of HPMC E50 was higher than CMC, HPMC E50 micelles were formed in the reaction system and further performed functions as template. The schematic description of this process was shown in Fig. 2. Since micelles in the solution provided attachment point for silica hydrolysis and polycondensation, silica frame formation that consisted of Si-O-Si can be accelerated. Silica frame deposited on the micelles and a certain time was required. Compared to B-SX, silica formation time of BM-SX was obviously shorter, demonstrating that the adding of HPMC E50 accelerated the speed of silica deposition. The reason can be ascribed to (1) the micelles in the system enlarged silica reaction surface and volume; (2) the system's viscosity increased owing to the adding of cellulose excipient.

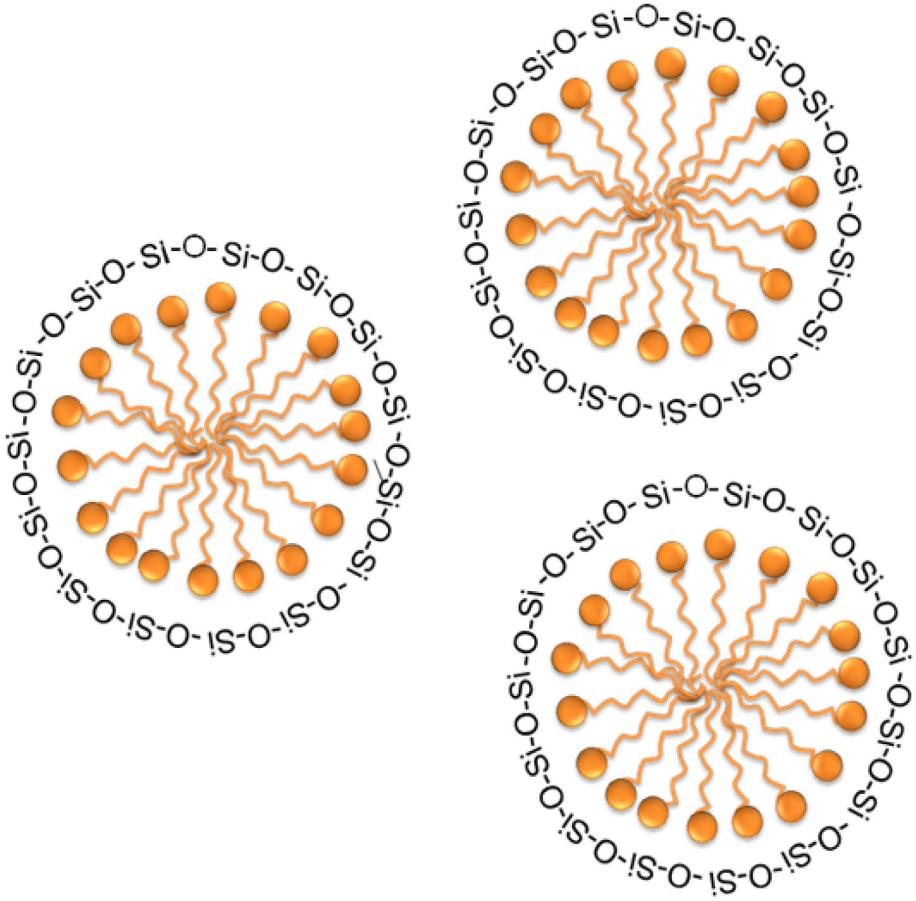

Fig. 2. Schematic illustration of reaction process for forming BM-SX.

3.2. Property characterization

According to Fig. 3A and B, both B-SX and BM-SX consisted of connective stacked particles. The surface of BM-SX exhibited many small pores while B-SX not, implying that HPMC E50 micelles were favorable for establishing pores in silica frame since these micelles functioned as templates.

In nitrogen adsorption/desorption isotherms of B-SX and BM-SX (see Fig. 3C and D), there was one hysteresis loop in the relative pressure of 0.6 to 1.0, demonstrating that both B-SX and BM-SX exhibited mesopores in silica frame. Compared to B-SX, there was another hysteresis loop in the relative pressure of 0.2 to 0.4, reflecting that there were extra mesopores in the silica frame of BM-SX [16,17]. It was obvious that HPMC E50 micelles contributed to the formation of these mesopores and the detection of these mesopores can be distinguished from other mesopores since the two hysteresis loops were clearly separated. With these extra mesopores, the mean pore diameter of BM-SX reached to 4.6 nm, which was larger than that of B-SX (3.8 nm). The specific surface area and pore volume of BM-SX were 568.49 cm^2/g and 0.47 cm^3/g respectively, which was also higher than B-SX (547.38 cm^2/g, 0.39 cm^3/g).

DSC experiment is one effective strategy to analyze drug crystalline state. In Fig. 4, DSC curve of NDP showed its single endothermic peak at 158.05 °C, which was its melting point, confirming that it was crystalline phase. However, no melting peak can be observed after loading NDP into either B-SX or BM-SX, demonstrating that NDP changed its crystalline phase to amorphous phase [18–20]. The amorphous phase of NDP had ability to enhance drug solubility owing to the improved energy provided by its amorphous phase, which can further increase drug dissolution and cellular transmembrane transport.

3.3. Drug dissolution

Drug loading capacity of NDP and B-SX and NDP and BM-SX were 10.34% and 9.76%, respectively. The drug loading capacity of NDP and BM-SX was a little lower than NDP and B-SX because the addition of HPMC E50 enhanced the weight of total carrier. NDP was quite poorly water-soluble evidenced by its low dissolution in vitro release test (see Fig. 5A) and its highest cumulative drug release was only almost 10%. The use of B-SX and BM-SX effectively enhanced NDP dissolution to more than 70% and 80% respectively owing to the fact that the crystalline state of NDP converted from crystal phase to amorphous phase and therefore improved NDP solubility energy [19,21]. Also, NDP was higher dispersed in the reaction system of B-SX and BM-SX and drug surface area can be enlarged, which was also favorable for drug dissolution. It should be noted that the burst release in NDP loaded BM-SX and NDP loaded B-SX occurred because drug released from the carrier when powered drug loaded carrier touched the medium. The carrier cannot delay drug release possibly because the located position of drug was not in the deep porous channels, which can be seen from other reported silica carriers [7]. The initial release (before 10 min) of NDP loaded B-SX was as fast as NDP loaded BM-SX because the loaded NDP was amorphous state in B-SX and BM-SX. However, the drug release reduction of NDP loaded B-SX was extremely obvious after 10 min (drug dissolution reduced to almost 40% at 60 min), showing that the a certain amount of dissolved amorphous NDP quickly changed to crystal NDP and the solubility of crystal NDP was quite low in the dissolution medium. This phenomenon was common for solid dispersions and considered to be a serious weakness for reducing the stability of drug delivery system. This defect can be avoided by applying BM-SX since the micelles were favorable for remaining high amorphous drug phase

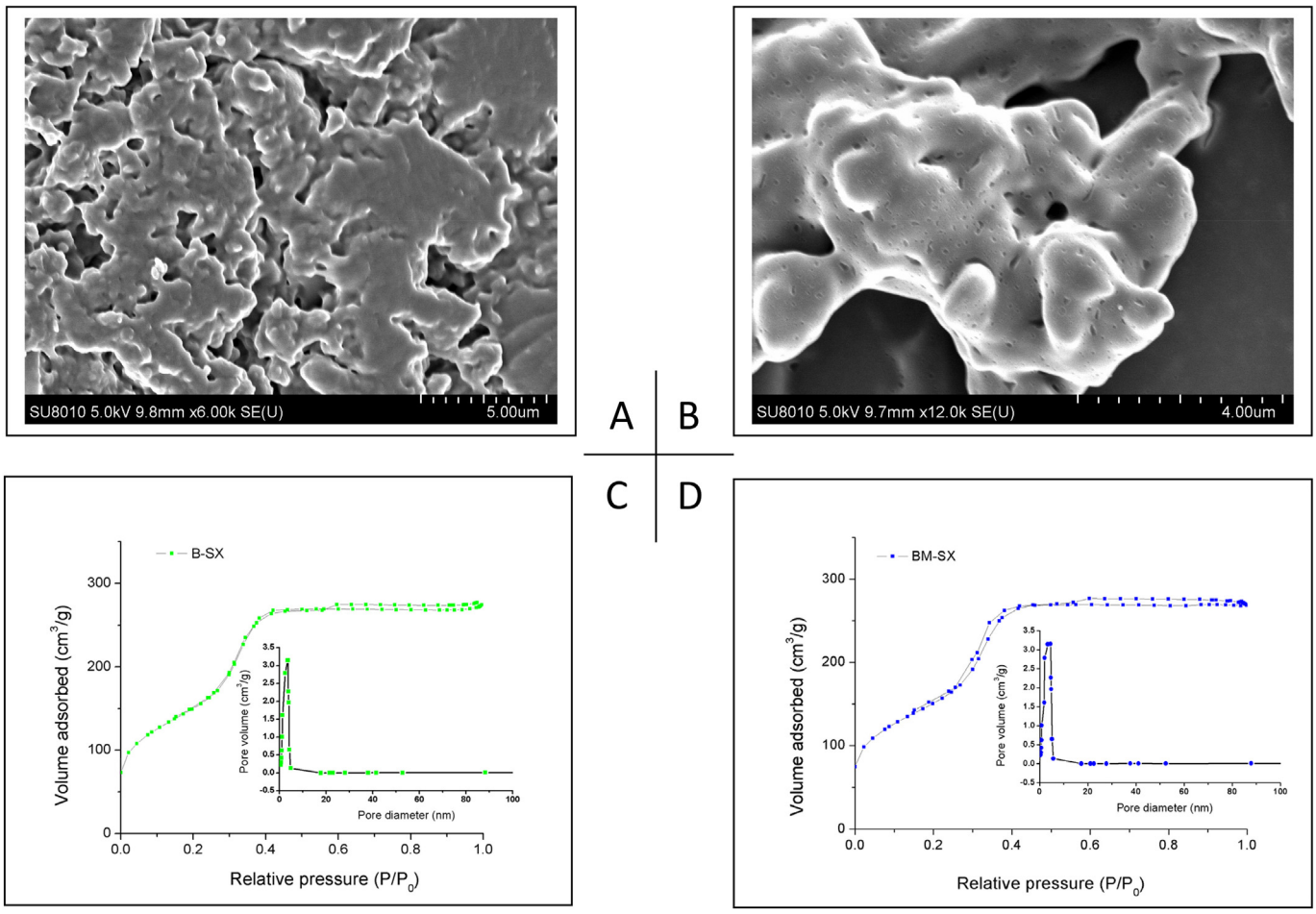

Fig. 3. A, SEM image of B-SX; B, SEM image of BM-SX; nitrogen adsorption/desorption result of B-SX; nitrogen adsorption/desorption result of BM-SX.

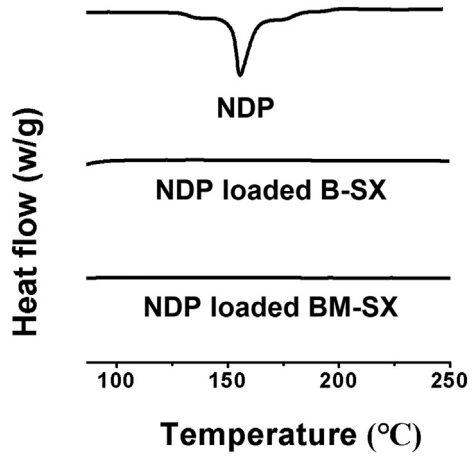

Fig. 4. DSC curves of NDP, NDP loaded B-SX and NDP loaded BM-SX.

and therefore no drug dissolution deduction can be observed after achieving highest cumulative drug release point.

3.4. Contact angle analysis

Contact angle measurement was one effective method to reflect the wetting property of samples [22]. Herein, dynamic contact angle tests of NDP, B-SX, BM-SX, NDP loaded B-SX and NDP loaded BM-SX were initially conducted (see Fig. 5B). The poorly water-soluble NDP presented the highest contact angles during dynamic contact angle process, showing that NDP was the hardest to be wetted [23,24]. The two carriers were easily to be wetted owing to their mesopores. The contact angles of BM-SX were lower than B-SX at any time point, illustrating that the extra mesopores formed due to HPMC E50 micelles contributed to its superior wetting property. After loading NDP into the two carriers, the contact angles of NDP loaded B-SX and NDP loaded BM-SX were obviously reduced compared to NDP but higher than corresponding carrier, which gave hints that (1) NDP loaded in the carrier was easier to be wetted than NDP because the loaded NDP was amorphous phase with high solubility according to DSC analysis result; (2) NDP loaded BM-SX had superior wetting property compared with NDP loaded B-SX since the pore diameter of BM-SX was larger than B-SX, which further improved its hydrophilicity; (3) contact angles of drug loaded carrier were higher than their corresponding carriers, showing that the wetting property ability decreased after loading drug into carriers because more time was required for wetting loaded drug other than wetting carrier.

After placing tablet samples in desiccator with humidity of 92.5% for 5 d, contact angles of NDP loaded B-SX (see Fig. 5C) were a litter higher than original data while NDP loaded BM-SX did not exhibit much differences, demonstrating that the wetting property of NDP loaded B-SX became worse because the system had poor stability and the loaded NDP was easier to convert amorphous phase to crystal phase after absorption of moisture. The wetting property reduction of NDP loaded B-SX was more obvious after being stored in desiccator with humidity of 92.5% for 10 d. On the contrary, the wetting property reduction of NDP loaded BM-SX almost had no differences between 5 d and 10 d. The above results confirmed the strong power of HPMC E50 micelles in maintaining amorphous NDP in the carrier since the

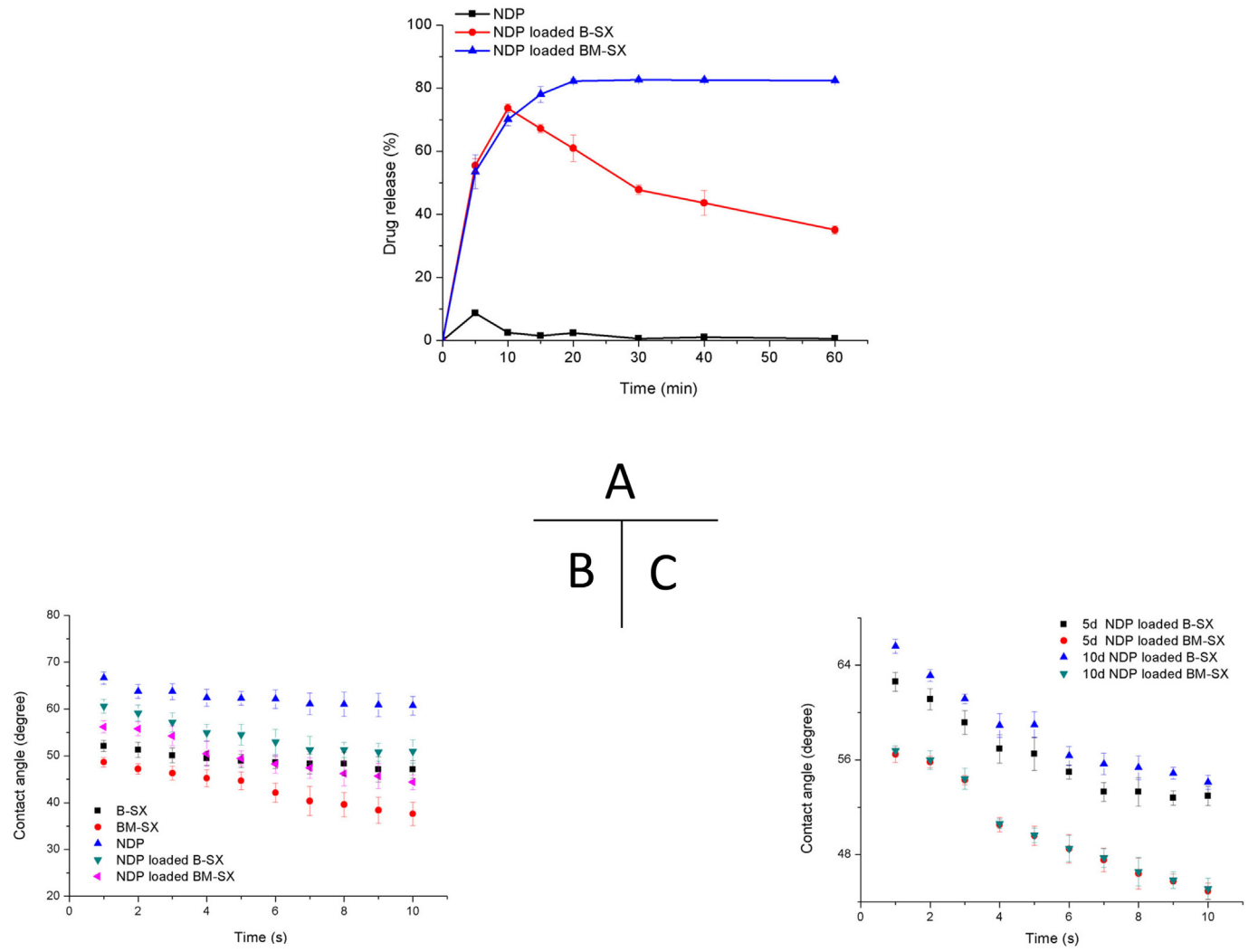

Fig. 5. A, Drug dissolution result; B, contact angle measurement of samples; C, contact angle measurement of samples after conducting moisture absorption.

Table 1
Mean Papp of NDP in the directions of AP → BL and BL → AP sides.

Samples	AP → BL	BL → AP	Efflux ratio
	Papp × 10^6 (cm/s)	Papp × 10^6 (cm/s)	
NDP	5.48	16.15	2.95
NDP + CsA	7.05	9.68	1.37
NDP loaded B-SX	8.67	10.24	1.18
NDP loaded BM-SX	14.29	9.26	0.65

micelles enhanced drug solubility and therefore the crystal NDP can never generate in the system. The superior stability of NDP loaded BM-SX was the outstanding advantage property among drug delivery systems established by mesoporous silica materials.

3.5. Cellular toxicity and transmembrane transport

Cellular toxicity of BM-SX and B-SX was conducted using caco-2 cells. As seen in the obtained result in Supporting information, BM-SX and B-SX had no cellular toxicity, demonstrating that the two carriers were safe to be used. According to Table 1, absorption apparent permeability of NDP loaded carrier was higher than NDP and NDP loaded BM-SX was better than NDP loaded B-SX, demonstrating that the two carriers displayed capacities in enhancing drug absorption permeability owing to the amorphous phase of loaded drug [25]. The contribution of BM-SX in performing superior drug absorption permeability can be ascribed to HPMC E50 micelles with ability to increase drug solubility. It was wide known that P-glycoprotein (p-gp), a drug transporter, is an energy-dependent drug efflux pump that has a wide range of subspecies and plays an important role in the absorption of many drugs. It relies on the energy released by the hydrolysis of ATP to transport the substrate from the cell to the extracellular, leading to a decrease in intracellular drug concentration. P-gp plays an important role in influencing oral bioavailability of drugs and inhibition of p-gp efflux can improve the permeability of drugs to cells and the absorption of drugs in cells and tissues. CsA is a classical P-gp inhibitor. When CsA is added to the transport medium, AP → BL transport increased while BL → AP transport decreased significantly. After loading NDP into B-SX and BM-SX, Papp(AP → BL) increased about 1.58 times and 2.61 times that of the NDP group, Papp(BL → AP) decreased by about 37% and 43% compared with the control group, and efflux ratio reduced by about 60% and 78% respectively. The experimental results showed that B-SX and BM-SX could exert function as drug efflux inhibitor to inhibit the efflux effect of p-gp drug pump, reduce the secretion and transport of NDP from the BL lateral AP side of caco-2 monolayer cell membrane, and promote the absorption and transport of NDP from the AP lateral BL side. The superior drug efflux inhibition ability of BM-SX also owed to HPMC E50 micelles. Therefore, BM-SX had huge value for establishing drug delivery systems.

4. Conclusion

The present work combined the advantages of micelles and biomimetic silica materials by obtaining BM-SX. B-SX without micelles was prepared as control, and NDP with poor water solubility was used as model drug. The content mainly focused on drug dissolution, systemic stability and cellular transmembrane transport of NDP loaded B-SX and NDP loaded BM-SX. The results demonstrated that the surface of BM-SX exhibited many small pores while B-SX not, implying that HPMC E50 micelles were favorable for establishing pores in silica frame. It was obvious that HPMC E50 micelles contributed to the formation of these mesopores and the detection of these mesopores can be distinguished from other mesopores since the two hysteresis loops were clearly separate. With these extra mesopores, the mean pore diameter, surface area and pore volume of BM-SX were all larger than B-SX. After loading NDP into the two carriers, crystal NDP changed to amorphous phase, leading to enhanced NDP dissolution. BM-SX presented superior abilities not only for its higher drug dissolution compared to B-SX but also for its capacity in remaining high amorphous drug phase and therefore no drug dissolution deduction can be observed after achieving highest cumulative drug release point. The contact angle measurement result after conducting moisture absorption confirmed the strong power of HPMC E50 micelles in maintaining amorphous NDP in the carrier. Both B-SX and BM-SX could increase drug absorption permeability and exert function as drug efflux inhibitor to inhibit the efflux effect of p-gp drug pump, reduce the secretion and transport of NDP from the BL lateral AP side of caco-2 monolayer cell membrane, and promote the absorption and transport of NDP from the AP lateral BL side. The superior drug efflux inhibition ability of BM-SX also owed to HPMC E50 micelles. Overall, BM-SX with outstanding abilities in enhancing drug dissolution, remaining high stability and improving cellular transmembrane transport appeared as novel mesoporous silica carrier for delivering poorly water soluble drug.

Supplementary data to this article can be found online at https://doi.org/10.1016/j.msec.2020.111372.

CRediT authorship contribution statement

Qiankun Jiang: Methodology; Lingqiong Wu: Formal analysis; Yue Zheng: Data curation; Xiaojie Xia: Validation; Ping Zhang: Writing – original draft; Tong Lu: Writing – original draft; Jing Li: Project administration, Writing – review & editing.

Declaration of competing interest

The authors declare that they have no known competing financial interests or personal relationships that could have appeared to influence the work reported in this paper.

References

[1] Y.L. Dechao Niu, Jianlin Shi, Chem. Soc. Rev. 46 (2017) 569–585.
[2] Z.L. Ling Zhang, Chao Kong, Chun Liu, Kuan Yang, Huijun Chen, a.F.Q. Jinfeng Huang, Small (2018) 1–13.
[3] X.F. Wenqiang Li, Xiaokun Wang, Xiaohong Shang, Qi Wangb, Juntang Lin, Z.L. Zhiguo Hu, Mater. Sci. Eng. C 91 (2018) 688–695.
[4] Geneviève Gaucher, Prashant Satturwar, Marie-Christine Jones, Alexandra Furto, J.-C. L., Eur. J. Pharm. Biopharm. 76 (2010) 147–158.
[5] T. Farías, L.C. de Ménorval, J. Zajac, A. Rivera, Colloids and Surfaces A: Physicochem. Eng. Aspects 345 (2009) 51–57.
[6] J. Aguiar, P. Carpena, J.A. Molina-Bolívar, C.C. Ruiz, J. Colloid Interface Sci. 258 (2003) 116–122.
[7] J. Li, L. Xu, H. Liu, Y. Wang, Q. Wang, H. Chen, W. Pan, S. Li, Int. J. Pharm. 467 (2014) 9–18.
[8] C.C. Lechner, C.F.W. B., Marine Drugs 13 (2015) 5297–5333.
[9] Katharina Lutz, Christian Gröger, M.S.a.E. Brunner, Phys. Chem. Chem. Phys. 7 (2005) 2812–2815.
[10] A. Bernecker, R. Wieneke, R. Riede, M. Seibt, A. Geyer, C. Steinem, J. Am. Chem. Soc. 132 (2010) 1023–1031.
[11] F.Z. Jiahua Zhou, Jing Li, Yongjun Wang, Mater. Sci. Eng. C 90 (2018) 314–324.
[12] C.S. Wei Lei, Tongying Jiang, Yikun Gao, Yang Yang, Qinfu Zhao, Siling Wang, Mater. Sci. Eng. C 105 (2019) 110103.
[13] Z.H. Na Fan, Pingping Ma, Xin Wang, Chang Li, Jin Sun, Yinghua Sun, Jing Li, Carbohydr. Polym. 181 (2018) 543–550.
[14] Gargi Basu Ray, Indranil Chakraborty, S.P. Moulik, J. Colloid Interface Sci. 294 (2006) 248–254.
[15] Mohammad Amin Mir, Oyais Ahmad Chat, Muzaffar Hussain Najar, Mohammad Younis, Aijaz Ahmad Dar, G.M. Rather, J. Colloid Interface Sci. 364 (2011) 163–169.
[16] J.Z. Yanzhuo Zhang, Tongying Jiang, Siling Wang, Int. J. Pharm. 410 (2011) 118–124.
[17] B. Tzankov, K. Yoncheva, M. Popova, A. Szegedi, G. Momekov, J. Mihály, N. Lambov, Microporous Mesoporous Mater. 171 (2013) 131–138.
[18] F. Uejo, W. Limwikrant, K. Moribe, K. Yamamoto, Asian Journal of Pharmaceutical Sciences 8 (2013) 329–335.
[19] C.A. McCarthy, R.J. Ahern, R. Dontireddy, K.B. Ryan, A.M. Crean, Expert Opinion on Drug Delivery 13 (2016) 93–108.
[20] Y. Wang, Q. Zhao, N. Han, L. Bai, J. Li, J. Liu, E. Che, L. Hu, Q. Zhang, T. Jiang, S. Wang, Nanomedicine 11 (2015) 313–327.
[21] T. Numpilai, S. Muenmee, T. Witoon, Mater. Sci. Eng. C 59 (2016) 43–52.
[22] Jing Li, Na Fan, Chang Li, Jian Wang, Sanming Li, Z. He, Appl. Surf. Sci. 420 (2017) 136–144.
[23] Jing Li, Na Fan, Xin Wang, Chang Li, Mengchi Sun, Jian Wang, Fu Qiang, Z. He, Eur. J. Pharm. Sci. 106 (2017) 244–253.
[24] Jing Li, Xin Wang, Chang Li, Na Fan, Jian Wang, Zhonggui He, J. Sun, Mol. Pharm. 14 (2017) 2781–2792.
[25] T.C. Mengmeng Yang, Lingchong Wang, Lihua Chen, Junsong Li, Liuqing Di, Colloids Surf. B: Biointerfaces 170 (2018) 187–193.
[26] Jing Fan, Qianjun He, Zhaokui Jin, Wei Chen, Weiren Huang, RSC Adv. 8 (2018) 14975–14982.

报告编号： 2022-0159

科 技 论 文 检 索 证 明

一、检索要求

检索 沈阳医学院（委托单位）李静（委托人）发表的科技论文被 Science Citation Index Expanded (SCI-EXPANDED)收录的情况及论文来源期刊在 Journal Citation Reports(JCR)中的影响因子、分区情况和中科院期刊分区（升级版）情况。

二、检索结果

经检索，李静 发表的如下 1 篇科技论文被 SCI 收录，情况如下：

Title: Biomimetic micellar mesoporous silica xerogel performs superior nitrendipine dissolution, systemic stability and cellular transmembrane transport
Author(s): Jiang, QK (Jiang, Qiankun); Wu, LQ (Wu, Lingqiong); Zheng, Y (Zheng, Yue); Xia, XJ (Xia, Xiaojie); Zhang, P (Zhang, Ping); Lu, T (Lu, Tong); Li, J (Li, Jing)
Source: MATERIALS SCIENCE & ENGINEERING C-MATERIALS FOR BIOLOGICAL APPLICATIONS Volume: 118 Article Number: 111372 DOI: 10.1016/j.msec.2020.111372 Published: JAN 2021
Accession Number: WOS:000600866900008
Document Type: Article
Addresses: [Jiang, Qiankun; Wu, Lingqiong; Zheng, Yue; Xia, Xiaojie; Zhang, Ping; Lu, Tong; Li, Jing] Shenyang Med Coll, Sch Pharm, Shenyang, Peoples R China.
Corresponding Address: Li, J (corresponding author), 146 Huanghe North St, Shenyang, Liaoning, Peoples R China.
E-mail Addresses: dddefghijklmn@163.com
ISSN: 0928-4931
eISSN: 1873-0191

JCR 分区：

序号	发文期刊	影响因子[2021]	JCR 类别	排序	JCR 分区
1	MATERIALS SCIENCE & ENGINEERING C-MATERIALS FOR BIOLOGICAL APPLICATIONS	8.457	MATERIALS SCIENCE, BIOMATERIALS	8/44	Q1

中科院期刊分区（升级版）：

序号	发文期刊	ISSN	大类	小类
1	MATERIALS SCIENCE & ENGINEERING C-MATERIALS FOR BIOLOGICAL APPLICATIONS	0928-4931	工程技术 2 区 top	MATERIALS SCIENCE, BIOMATERIALS 材料科学：生物材料 2 区

检索员：陈俊峰　　出具报告单位：中国科学院文献情报中心沈阳科技查新服务站

审核员：王东博　　完成时间：2022 年 07 月 11 日